The Astronomical Journal, 145:159 (8pp), 2013 June doi:10.1088/0004-6256/145/6/159

THE LAMOST SURVEY OF BACKGROUND QUASARS IN THE VICINITY OF THE ANDROMEDA AND TRIANGULUM GALAXIES. II. RESULTS FROM THE COMMISSIONING OBSERVATIONS AND THE PILOT SURVEYS

Zhi-Ying Huo[1], Xiao-Wei Liu[2,3], Mao-Sheng Xiang[3], Hai-Bo Yuan[2,8], Yang Huang[3], Hui-Hua Zhang[3], Lin Yan[4], Zhong-Rui Bai[1], Jian-Jun Chen[1], Xiao-Yan Chen[1], Jia-Ru Chu[5], Yao-Quan Chu[5], Xiang-Qun Cui[6], Bing Du[1], Yong-Hui Hou[6], Hong-Zhuan Hu[5], Zhong-Wen Hu[6], Lei Jia[1], Fang-Hua Jiang[6], Ya-Juan Lei[1], Ai-Hua Li[6], Guang-Wei Li[1], Guo-Ping Li[6], Jian Li[1], Xin-Nan Li[6], Yan Li[7], Ye-Ping Li[6], Gen-Rong Liu[6], Zhi-Gang Liu[5], Qi-Shuai Lu[6], A-Li Luo[1], Yu Luo[1], Li Men[1], Ji-Jun Ni[6], Yong-Jun Qi[6], Zhao-Xiang Qi[7], Jian-Rong Shi[1], Huo-Ming Shi[1], Shi-Wei Sun[1], Zheng-Hong Tang[7], Yuan Tian[1], Liang-Ping Tu[1], Dan Wang[1], Feng-Fei Wang[1], Gang Wang[1], Jia-Ning Wang[6], Lei Wang[6], Shu-Qing Wang[1], You Wang[6], Yue-Fei Wang[6], Ming-Zhi Wei[1], Yue Wu[1], Xiang-Xiang Xue[1], Zheng-Qiu Yao[6], Yong Yu[7], Hui Yuan[1], Chao Zhai[5], En-Peng Zhang[1], Hao-Tong Zhang[1], Jian-Nan Zhang[1], Wei Zhang[1], Yan-Xia Zhang[1], Yong Zhang[6], Zhen-Chao Zhang[6], Gang Zhao[1], Ming Zhao[7], Yong-Heng Zhao[1], Fang Zhou[6], Xin-Lin Zhou[1], Yong-Tian Zhu[6], and Si-Cheng Zou[1]

[1] Key Laboratory of Optical Astronomy, National Astronomical Observatories, Chinese Academy of Sciences, Beijing 100012, P. R. China; zhiyinghuo@bao.ac.cn
[2] Kavli Institute for Astronomy and Astrophysics, Peking University, Beijing 100871, P. R. China
[3] Department of Astronomy, Peking University, Beijing 100871, P. R. China
[4] Infrared Processing and Analysis Center, California Institute of Technology, MS 100-22, Pasadena, CA 91125, USA
[5] University of Science and Technology of China, Hefei 230026, P. R. China
[6] Nanjing Institute of Astronomical Optics & Technology, National Astronomical Observatories, Chinese Academy of Sciences, Nanjing 210042, P. R. China
[7] Shanghai Astronomical Observatory, Chinese Academy of Sciences, Shanghai 200030, P. R. China
Received 2012 November 5; accepted 2013 April 7; published 2013 May 10

ABSTRACT

We present new quasars discovered in the vicinity of the Andromeda and Triangulum galaxies with the Large Sky Area Multi-Object Fiber Spectroscopic Telescope, also named the Guoshoujing Telescope, during the 2010 and 2011 observational seasons. Quasar candidates are selected based on the available Sloan Digital Sky Survey, Kitt Peak National Observatory 4 m telescope, Xuyi Schmidt Telescope Photometric Survey optical, and *Wide-field Infrared Survey Explorer* near-infrared photometric data. We present 509 new quasars discovered in a stripe of $\sim$135 deg^2 from M31 to M33 along the Giant Stellar Stream in the 2011 pilot survey data sets, and also 17 new quasars discovered in an area of $\sim$100 deg^2 that covers the central region and the southeastern halo of M31 in the 2010 commissioning data sets. These 526 new quasars have *i* magnitudes ranging from 15.5 to 20.0, redshifts from 0.1 to 3.2. They represent a significant increase of the number of identified quasars in the vicinity of M31 and M33. There are now 26, 62, and 139 known quasars in this region of the sky with *i* magnitudes brighter than 17.0, 17.5, and 18.0, respectively, of which 5, 20, and 75 are newly discovered. These bright quasars provide an invaluable collection with which to probe the kinematics and chemistry of the interstellar/intergalactic medium in the Local Group of galaxies. A total of 93 quasars are now known with locations within 2.°5 of M31, of which 73 are newly discovered. Tens of quasars are now known to be located behind the Giant Stellar Stream, and hundreds are behind the extended halo and its associated substructures of M31. The much enlarged sample of known quasars in the vicinity of M31 and M33 can potentially be utilized to construct a perfect astrometric reference frame to measure the minute proper motions (PMs) of M31 and M33, along with the PMs of substructures associated with the Local Group of galaxies. Those PMs are some of the most fundamental properties of the Local Group.

Key words: galaxies: individual (M31, M33) – quasars: emission lines – quasars: general

Online-only material: color figures, machine-readable and VO tables

1. INTRODUCTION

Being the most luminous member of the Local Group and the nearest archetypical spiral galaxy, M31 serves as the best astrophysical laboratory for the studies of the physical and astrophysical processes that govern the structure, kinematics and the formation and evolution of distant galaxies. Recent deep optical surveys have revealed complex substructures within hundreds of kiloparsecs (kpc) of M31, with some of them stretching from M31 all the way to M33, which is about 200 kpc from M31, suggesting a possible recent close encounter of the two galaxies (Ibata et al. 2007; McConnachie et al. 2009). Detailed chemical and kinematic investigations of M31 and associated substructures are vital for our understanding of M31, and also for the theory of galaxy formation and evolution in general.

Finding background quasars in the vicinity of M31 have the two following potential important applications. First, the background quasars can serve as an ideal reference frame which would allow highly accurate astrometric measurement of the minute proper motion (PM) of M31 and also the PMs of its associated coherent substructures. Second, absorption-line spectroscopy of bright background quasars can be used to probe the distribution, chemical composition, and kinematics of the interstellar medium (ISM) of M31, the Milky Way, and the intergalactic medium (IGM) of the Local Group of galaxies. This technique can be used to probe structures further out from the center of the galaxy than would be possible with traditional

[8] LAMOST Fellow

stellar spectroscopy, or using H I 21 cm observations. In addition, M31 has always been a focus of interest for astronomical observations. Extensive photometric data spanning tens of years exist. Therefore, identifying background quasars in the vicinity of M31 should also enable the construction of a valuable sample for studying quasar variability.

The PM of M31 represents one of the most fundamental quantities of the Local Group, and its accurate measurement is vital to the study of the formation, evolution, and dynamics of the Local Group, in particular for quantifying the dark matter content. M31 is known to be located at a distance of ∼785 kpc (McConnachie et al. 2005), and is moving toward the Milky Way with a velocity of 117 km s^{-1} (Binney & Tremaine 1987, p. 605). However, its transverse velocity has remained unknown for a long time. The Very Long Baseline Array, with a PM measurement uncertainty of the order of 1 microarcsec, has measured the distance and PM of M33 by water maser observations (Brunthaler et al. 2005). However, water maser sources in M31 have been discovered only recently (Darling 2011); thus we do not yet have a long enough time baseline for a meaningful PM measurement. Based on kinematic information about M31's satellite galaxies, M33 and IC10, Loeb et al. (2005) and van der Marel & Guhathakurta (2008) deduced theoretical estimates for the PM of M31 of about 80 km s^{-1} (20 μas yr^{-1}). Sohn et al. (2012) presented the first direct PM measurements for three M31 fields (∼2.7 × 2.7 $arcmin^2$ for each field) using *Hubble Space Telescope* observations that span a time baseline of 5–7 yr. Due to the sparseness of known background quasars, their analysis had to resort to using compact background galaxies as reference sources, even though it was hard to obtain highly accurate positions for those galaxies given their nature as extended sources. Being essentially point sources with zero PMs, background quasars can serve as perfect reference sources for highly accurate PM measurements, provided that enough of them with sufficient space density can be identified.

At the distance of M31, even a luminous red giant branch star has an *I* magnitude fainter than 20, and hence high-resolution spectroscopic determinations of their chemical composition are no easy tasks even for a 10 m class telescope (Ibata et al. 2005; Gilbert et al. 2009). Absorption-line spectroscopy of background quasars allows one to probe the distribution, chemical composition, and kinematics of the ISM associated with M31, and this technique can be used to probe material further out from the galaxy center than is possible with traditional stellar spectroscopy or with H I 21 cm observations (Chemin et al. 2009). A number of papers have been published (see Savage et al. 2000; Schneider et al. 1993 and references therein), reporting Milky Way absorption-line systems which were detected in quasar spectra. Analyses of those systems have revealed great complexity of the Milky Way halo gas, which exhibits a wide range of ionization states, chemical compositions, and kinematics. Similar absorption-line spectroscopic analysis of M31 background quasars will help understand the formation history of M31 and the Local Group.

A number of efforts have been taken to search for background quasars behind nearby galaxies, with the intended purpose being to study their PMs or ISM/IGM. Tinney et al. (1997) and Tinney (1999) obtained a sample of quasars behind the Milky Way satellite galaxies. Kim et al. (2012) published 663 background quasar candidates in the Large Magellanic Cloud (LMC), Kozłowski et al. (2012; see also references therein) increased the number of known background quasars to 200 behind the southern edge of the LMC. For M31, Crampton et al. (1997) presented several quasar candidates. Until recently, Sloan Digital Sky Survey (SDSS; York et al. 2000) obtained 75 low-redshift quasars in three spectroscopic plates in two fields in the outer halo of M31 (cf. Adelman-McCarthy et al. 2006, 2007). As far as we are aware, since 2007 no further observations targeting quasars around M31 have been made by SDSS. In the first of this series of papers we presented 14 new quasars discovered with the Large Sky Area Multi-Object Fiber Spectroscopic Telescope (LAMOST) during its early commissioning phase (see Huo et al. 2010, hereafter Paper I).

LAMOST is a quasi-meridian reflecting Schmidt telescope with an effective aperture of about 4 m and a field of view of 5° in diameter (Wang et al. 1996; Su et al. 1998; Xing et al. 1998; Zhao 2000; Cui et al. 2004, 2010, 2012; Zhu et al. 2006, see http://www.lamost.org/website/en/). Recording 4000 celestial object spectra simultaneously with a parallel fully controllable fiber positioning system, LAMOST is the telescope with the highest rate of spectral acquisition at the present time. After a period of two years of commissioning for the purpose of technical fine-tuning, performance characterization and optimization, as well as scientific capability demonstration, the LAMOST pilot surveys were initiated in 2011 October and completed in spring the following year (see Zhao et al. 2012). In this paper, we report newly discovered background quasars in the vicinity of M31 and M33, based on LAMOST data obtained during the commissioning phase of 2010 as well as during the pilot surveys from autumn 2011 to spring 2012.

2. CANDIDATE SELECTION

With the aim of searching for background quasars in the vicinity of M31 and M33, we selected quasar candidates based on the available optical, near-infrared (IR) photometric data in the extended area of M31 and M33. Only point-source quasar candidates were selected in order to provide a clean sample for the PM measurements and ISM/IGM studies.

Figure 1 shows the fields observed with the LAMOST during 2010 and 2011 observational seasons. M31 is covered by a special scan of a total area of 100 deg^2, 5° wide and 20° long, along the northeast–southwest direction (Adelman-McCarthy et al. 2006, 2007). M33 is covered by the SDSS southern Galactic cap survey (Aihara et al. 2011). Following Richards et al. (2002), low-redshift quasar candidates are selected as outliers from the stellar loci on the SDSS color–color diagrams (see also Paper I for the color–color diagrams and selection criteria). The candidates are required to have magnitude errors less than 0.2 mag in *ugriz*. With a magnitude limit set at $i \leqslant 20.0$, the low-redshift quasar candidates thus selected have a number density of 27 deg^{-2}.

As shown in Figure 1, there are no reliable photometric data from the SDSS in the central area of M31 and M33 given the very high stellar densities there. To select candidates in those crowded fields, we have made use of the *UBVRI* photometric catalog of M31 and M33 provided by the Kitt Peak National Observatory (KPNO) 4 m telescope (Massey et al. 2006). In doing so, we convert the KPNO *UBVRI* magnitudes to the SDSS *ugriz* using the transformations provided by Jester et al. (2005) for quasars of redshifts $z \leqslant 2.1$.

In addition to those purely optically selected candidates, we have selected quasar candidates combining the optical and IR photometry. Sources from *Wide-field Infrared Survey Explorer* (*WISE*; Wright et al. 2010) with colors $W1 - W2 > 0.8$ were selected (see Figures 11 and 12 in Yan et al. 2013 for the color–color distributions of different source

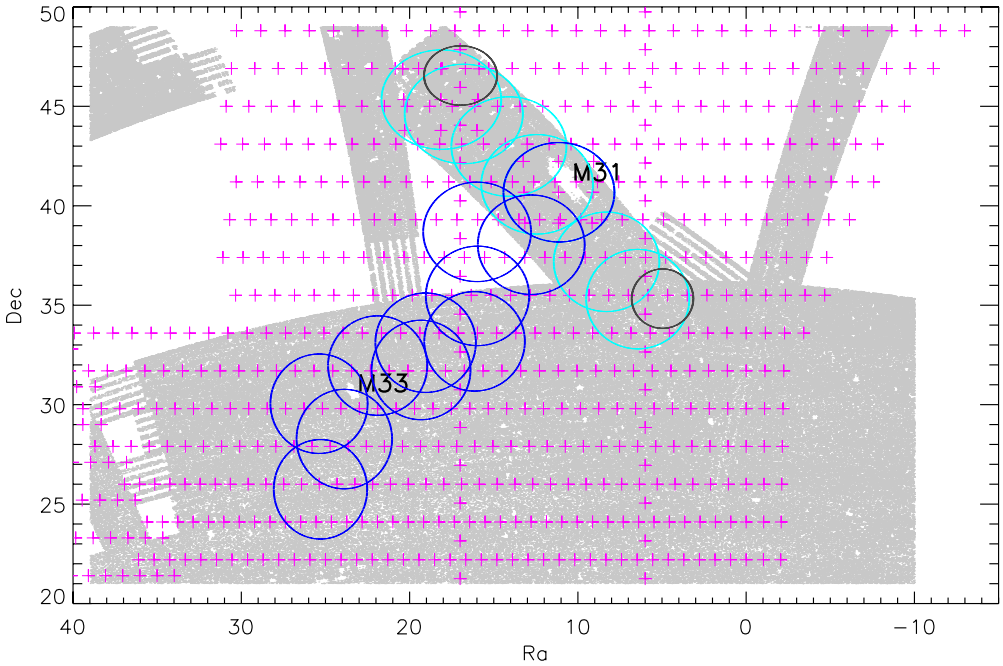

Figure 1. Fields observed with the LAMOST in the vicinity of M31 and M33 during the 2010 and 2011 observational seasons. The positions of M31 and M33 are labeled with characters, M31 and M33 are centered in the white areas. The gray area represents the SDSS footprint in this area. The magenta plus symbols delineate the centers of the individual XSTPS fields covered the M31/M33 area, with 2×2 deg^2 for each field. The cyan and blue circles represent the LAMOST fields observed in 2010 and 2011, respectively. The black circles represent the three SDSS spectroscopic fields targeting quasar candidates, the two plates in the northeast halo have the same central positions.

(A color version of this figure is available in the online journal.)

classification; also Stern et al. 2012; Wu et al. 2012 and references therein) and cross-correlated with the optical point-source catalogs of SDSS, KPNO, and the Xuyi Schmidt Telescope Photometric Survey (XSTPS; X.-W. Liu et al., in preparation; see also http://kiaa.pku.edu.cn/DSSGAC/overview.html). XSTPS has a component that extends to the M31/M33 area, as shown in Figure 1. In total, about 26 quasar candidates per square degree were selected by this technique for a limiting magnitude $i \leqslant 20.0$. For the sky area also covered by SDSS, we find that about 60% of these *WISE*-IR quasar candidates overlap with the optically selected low-redshift sample. As shown in Wu et al. (2012), this IR-based technique is capable of finding quasars with redshifts up to $z < 3.5$.

On the other hand, for the central regions of M31 and M33, this IR selection algorithm also yields too many interlopers, in particular along the optical disk of M31 and M33. We expect that most of these sources are actually candidates asymptotic giant branch stars, planetary nebulae, young stellar objects, or red stars. These are interesting objects to study in their own right. Furthermore, finding quasars in the very central regions of M31 and M33 will be extremely valuable for the PM measurements and ISM spectroscopic studies. As such we have included all those candidates in our input catalogs for LAMOST observations. The cyan and blue circles in Figure 1 represent the LAMOST fields observed during the 2010 and 2011 observational seasons; the sky area covered during each year was ∼100 deg^2 and ∼135 deg^2, respectively. In 2010, only optically selected low-redshift quasar candidates based on the SDSS colors were selected.

3. OBSERVATIONS AND DATA REDUCTION

M31 has been targeted by the LAMOST since the commissioning phase initiated in 2009. Paper I presented some of the early results about background quasars discovered by LAMOST. Here we present results based on data collected in the 2010 and 2011 observational seasons.

The exposure time for the plates varies from 600 to 1800 s, repeated two or three times to allow rejection of cosmic rays and to increase the signal-to-noise ratio (S/N). In total, 731 and 5641 unique quasar candidates were observed in 2010 and 2011, respectively. Some sources were targeted repeatedly. This is partly because the field of view of LAMOST is circular, which forces adjacent fields to overlap to allow coverage of a large contiguous sky area. In 2010, only SDSS optically selected low-redshift quasar candidates were selected and observed. In 2010 October and November, LAMOST CCDs suffered severe electromagnetic interference and insufficient dewar cooling, and so few useful data were collected. See Figure 1 for the fields targeted by the LAMOST in both 2010 and 2011.

The LAMOST has 16 low-resolution spectrographs, each accommodating 250 fibers. From the fall of 2011, LAMOST implemented slit masks with a width of 2/3 the 3.3 arcsec fiber diameter, yielding a spectral resolving power ∼1800. Before that a mixture of full (i.e., no slit masks) and 1/2 slit modes were used, but mostly in full slit mode, which yields a spectral resolution ∼1000. The light that enters each spectrograph is split into two channels, the blue and red channels, for which the wavelength coverages are 3700–5900 Å and 5700–9000 Å, respectively. The spectra from each spectrograph are imaged onto two 4096 × 4096 CCD cameras (see Cui et al. 2012 for further details). The spectra were reduced using the LAMOST two-dimensional (2D) pipeline, including bias subtraction, spectra tracing and extraction, wavelength calibration, flat fielding, and sky subtraction (see Luo et al. 2004, 2012). Considering the uncertainties in the commissioning phase and the pilot surveys, and the relatively low S/N of most quasar candidate spectra, for the current work of identifying quasars, the non-flux-calibrated

Table 1
Catalog of New Quasars in the Vicinity of M31 and M33 Discovered by LAMOST in Fields Observed in 2010 and 2011

Object	R.A.	Decl. (J2000)	Redshift	*u*	*g*	*r*	*i*	*z*	*A*(i)	Selection
J003255.71+394619.2	8.232129	39.772018	1.134	···	18.53	18.24	18.29	···	0.12	W, -, -
J003432.52+391836.1	8.635497	39.310022	0.138	18.55	18.53	18.38	17.87	18.03	0.10	-, S, M
J003459.61+420655.2	8.748376	42.115341	2.472	···	18.86	18.60	18.71	···	0.12	W, -, -
J003506.69+404003.4	8.777890	40.667629	1.844	20.27	20.05	19.91	19.56	19.43	0.14	-, S, -
J003514.29+401414.6	8.809581	40.237413	0.279	···	19.50	18.74	18.57	···	0.12	W, -, -
J003522.68+393353.9	8.844538	39.564987	0.670	···	19.32	19.48	19.53	···	0.13	W, -, -
J003524.49+394619.1	8.852052	39.771992	2.340	···	19.25	19.03	18.77	···	0.12	W, -, -
J003535.01+404351.2	8.895891	40.730891	1.774	20.33	20.21	20.25	19.90	20.12	0.13	-, S, -
J003546.45+413358.6	8.943565	41.566297	2.580	···	19.21	18.93	19.02	···	0.14	W, -, -
J003619.34+411746.5	9.080616	41.296262	1.651	20.38	19.90	19.56	19.21	19.09	0.14	-, S, -

Notes. W represents candidates selected by the IR criteria based on the *WISE* data, S represents those optically selected with the SDSS criteria for low-redshift quasars, and M represents those optically selected from the KPNO 4 m Local Group Galaxy survey data (Massey et al. 2006). The table contains information about 526 new quasars.

(This table is available in its entirety in machine-readable and Virtual Observatory (VO) forms in the online journal. A portion is shown here for guidance regarding its form and content.)

spectra were used. Hence the photometric magnitudes serve as much better measurements of the brightness of our targets.

4. RESULTS AND DISCUSSION

This current work is based on observations collected during the LAMOST commissioning phase and the pilot surveys when the LAMOST performance was still being characterized and optimized. Thus it is unavoidable that the data presented here suffer from some defects in one way or another, such as low throughput, poor sky subtraction, and so on. The fiber positioning, although improved significantly in spring 2011, still has room for further improvement. Fortunately, given their characteristic broad emission line, quasars are easily identified. We visually examined the one-dimensional spectra of each individual quasar candidate. We required that at least two emission lines were securely identified. The results led to the discovery of 17 and 509 new quasars in the vicinity of M31 and M33 in the fields observed in 2010 and 2011, respectively. If we adopt a luminosity cut following the SDSS Quasar Survey (Schneider et al. 2010, see also the references therein), with absolute magnitude $M_i = -22.0$ in a cosmology $H_0 = 70$ km s^{-1} Mpc^{-1}, $\Omega_{\rm M} = 0.3$, and $\Omega_\Lambda = 0.7$, then the number of newly discovered quasars are 15 and 509 in 2010 and 2011 data sets, respectively.

All the new quasars have reasonable S/N and at least two identified emission lines, thereby allowing reliable redshift estimates (see Figure 2). In Table 1, we present the catalog of these newly discovered quasars. The properties of these quasars, including target names (in the format of Jhhmmss.ss+ddmmss.s), equatorial coordinates, redshifts, the observed SDSS *u*, *g*, *r*, *i*, *z* magnitudes without extinction corrections, *i*-band extinction from Schlegel et al. (1998), and the selection criteria, are listed. Only a portion of the table is shown here. The whole table, containing information about all 526 new quasars, is available in the online journal. In the last column of Table 1, W indicates candidates selected with the IR criteria based on the *WISE* data, S indicates those optically selected using the SDSS criteria for low-redshift quasars, and M indicates those optically selected candidates based on the data from the KPNO survey of Local Group Galaxies. Columns 5–9 give the SDSS *u*, *g*, *r*, *i*, *z* magnitudes. For some targets only the *g*, *r*, *i* magnitudes are given. Those are targets selected by cross-correlating the *WISE*-IR candidates with the XSTPS optical catalog. Figure 2 shows spectra of seven new quasars spanning a wide range of redshifts. The spectra have not been flux calibrated. At wavelengths shorter than 4000 Å, where the instrument throughputs are low, as well as between the dichroic crossover wavelength range 5700–6000 Å, large spike- and trough-like artifacts often appear in the flux-calibrated spectra. This is particularly true for spectra with relatively low S/N, as is the case for many of our targets of interest here. Because of this, we have opted to not to use the flux-calibrated spectra. Since the LAMOST spectra were oversampled, we binned the spectra by a factor of four to improve the S/N. Cosmic rays which remained after pipeline processing were removed manually for clarity. The catalog and the individual spectra are available at the LAMOST public Web site http://www.lamost.org.

In addition to the 526 confirmed quasars, another 20 and 193 "probable" quasars have been identified in the current LAMOST 2010 and 2011 data sets. They either have marginal S/N or have only one emission line detected and so are at uncertain redshifts. Further observations are needed to confirm their identifications. We take this "probable" quasar catalog as a supplemental list, this supplemental list and the related spectra are also available at the aforementioned Web site, which will be updated in real time as new data are obtained or the pipeline is improved. Finally, 11 and 23 previously known quasars are re-observed in the LAMOST 2010 and 2011 data sets, respectively.

The sample has a magnitude limit of $i = 20.0$. Among the 526 newly discovered quasars, the brightest, J010415.77+402243.9, has an *i* magnitude 15.45 with redshift of 0.193, and was previously unknown (its spectrum is shown in Figure 2). There are 5/20/75 new quasars brighter than 17.0/17.5/18.0 mag in *i* band, respectively. For comparison, among the quasars discovered in the three SDSS spectroscopic plates (Adelman-McCarthy et al. 2006, 2007) and in the LAMOST 2009 commissioning observations, the corresponding numbers are 1/1/12. Within a 10° radius of M31 and of M33, there are 155 previously known quasars with redshift estimates reported in the NED archive (see also Figure 6). Many of them have multiple photometric measurements taken in a variety of filters, and 151 of them fall in the area covered by the SDSS or XSTPS surveys. Using a 3″ cross-correlation radius, we searched their counterparts in the SDSS and XSTPS sources with *i* magnitudes brighter than 21.0 and 20.0, respectively. We find 116 of them

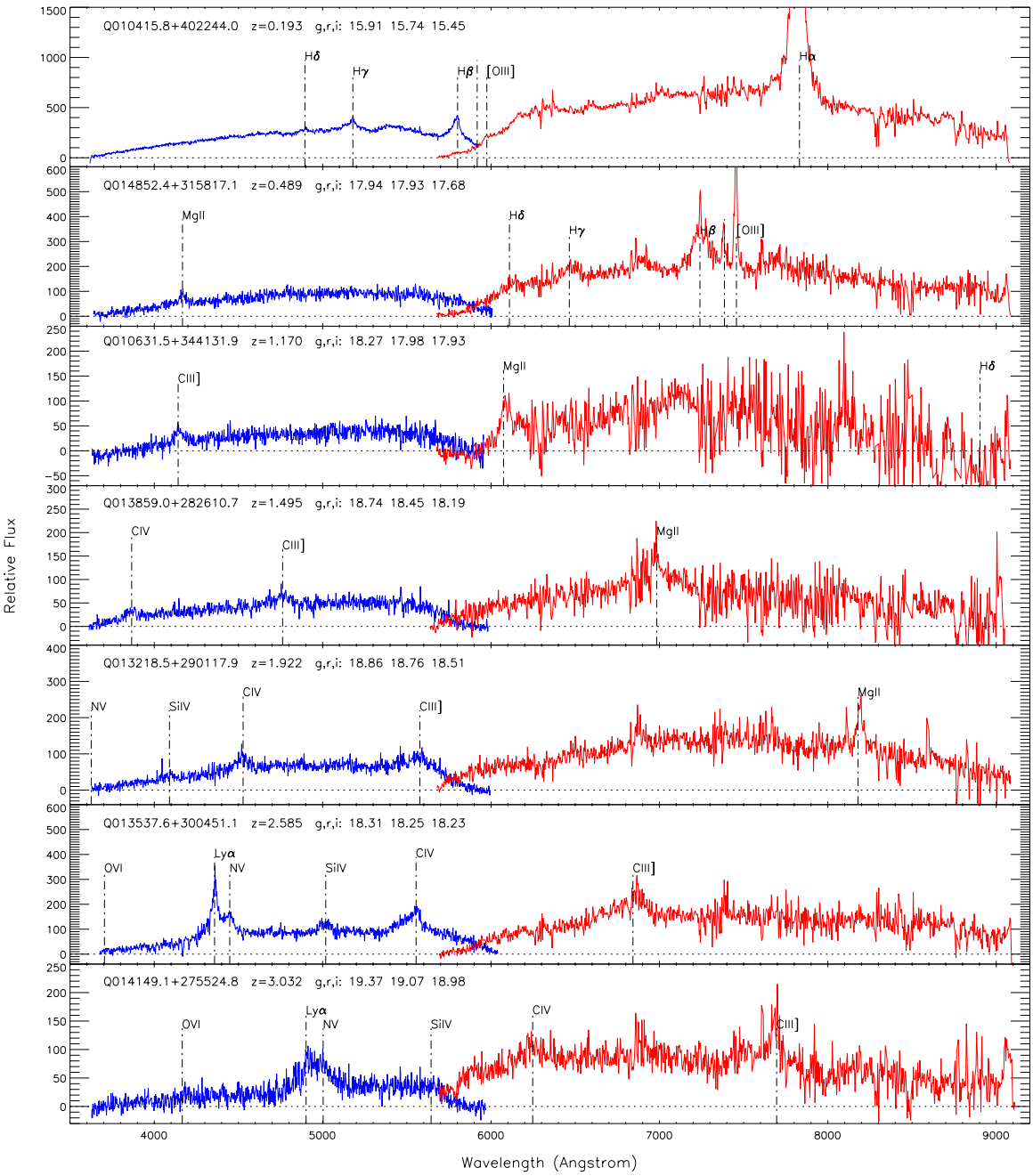

Figure 2. Example of LAMOST spectra of newly discovered quasars, with identified lines labeled. The relative flux is in units of counts per pixel, the horizontal dotted line labeled the zero flux. The spectra were binned by a factor of four, and remaining cosmic rays after pipeline processing were removed manually for clarity. (A color version of this figure is available in the online journal.)

have *i*-band counterparts, among them there are 20/41/52 quasars brighter than 17.0/17.5/18.0 mag, respectively. These bright quasars will serve as good candidates for absorption-line spectroscopic studies of the ISM of M31, M33 and of their related substructures. Figure 3 shows the magnitude distributions of the 532 quasars detected in the 2011 data sets, including 509 newly discovered quasars and 23 previously known sources which were re-observed by LAMOST. The magnitude has a bin size of 0.1, the *y*-axis is in quasar number density. In the magnitude distributions, as well as the following redshift distributions, only quasars detected in $\sim$135 deg^2 in 2011 are included, the quasars detected in 2010 are not considered. The magnitude distributions of the SDSS DR7 quasars (Schneider et al. 2010) are also shown for comparison. We can see that a large number of quasars with *i* magnitude fainter than 18.0 are left out by LAMOST due to its relatively low performance during the commissioning and pilot survey phases.

Figure 4 shows the redshift distributions of the 532 quasars detected by LAMOST in 2011. The redshift has a bin size of 0.1, the *y*-axis is in quasar number density, as in Figure 3. The lowest redshift is found for J003842.80+384551.9, at $z = 0.093$, while the highest redshift object is J011118.08+325833.8, at $z = 3.204$. For the optical selection criteria adopted here, low-redshift quasars selected as outliers of stellar loci on the SDSS color–color diagrams are mainly $z \leqslant 2.2$ quasars

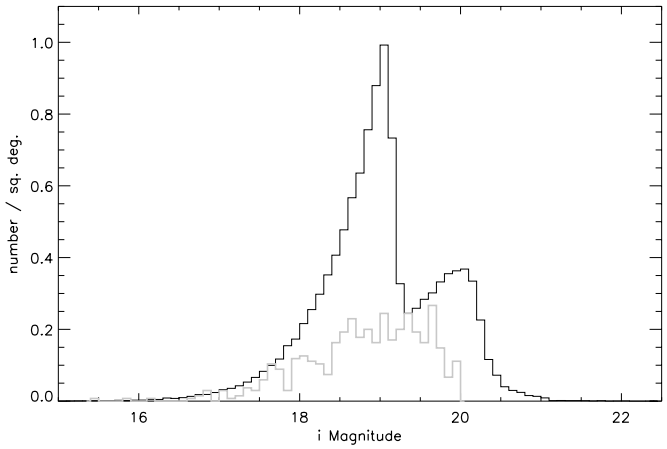

Figure 3. *i*-band magnitude distributions of the 532 quasars detected by LAMOST in 2011 (gray), including 509 newly discovered and 23 previously known quasars detected by LAMOST. The *i*-band magnitude distributions of the SDSS DR7 quasars are shown here for comparison (black), the steep gradients at $i \approx 19.1$ and $i \approx 20.2$ are due to the magnitude limits of the SDSS selection algorithms for the low- and high-redshift quasars. The magnitude bin size is set to 0.1. The *y*-axis is displayed in quasar number density.

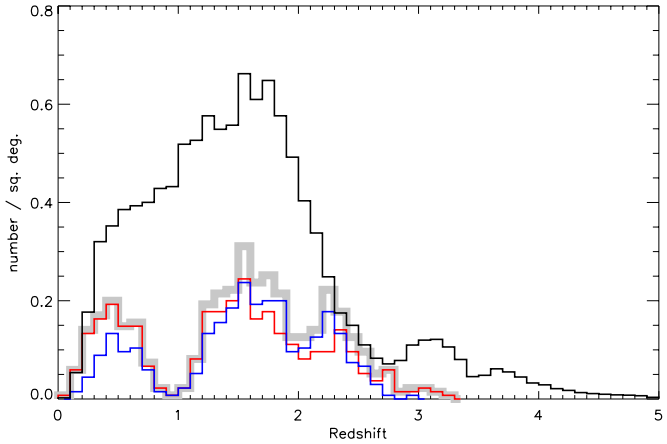

Figure 4. Redshift distributions of the 532 LAMOST detected quasars in 2011 (thick gray). The blue and red lines represent redshift distributions of SDSS low-redshift and optical/IR selected quasars, respectively. The redshift distributions of the SDSS DR7 quasars are also shown here for comparison (black), the low number density at $z \sim 2.7$ is caused by the degeneracy of the SDSS color of stars and colors of quasars near this redshift. The redshift bin size is set to 0.1. The *y*-axis is displayed in quasar number density.

(A color version of this figure is available in the online journal.)

(Fan 1999; Richards et al. 2001), whereas the optical/IR algorithm is capable of finding quasars of redshifts up to $z < 3.5$ (Wu et al. 2012). We note that there is no significant difference in redshift distribution between the optical and optical/IR selected quasars, as illustrated by the blue and red lines in Figure 4, respectively. For comparison, we also plot the redshift distributions of SDSS DR7 quasars. Except for the relatively lower number density in redshift space, we can also clearly see that there are two troughs in the redshift distributions of LAMOST detected quasars (see Figure 4), one near redshift ∼0.9 and another near ∼2.1. These are entirely due to the selection effects. For redshift $z < 0.9$, the Mg II λ2800, Hδ, Hγ, Hβ, and Hα, as well as the forbidden lines [O III] λ4959 and λ5007 all fall within the LAMOST wavelength coverage. For redshifts $1.1 < z < 2.0$, the C IV λ1549, C III] λ1908, and Mg II λ2800 lines are redshifted into the LAMOST wavelength range. For redshifts $z > 2.1$, Lyα and

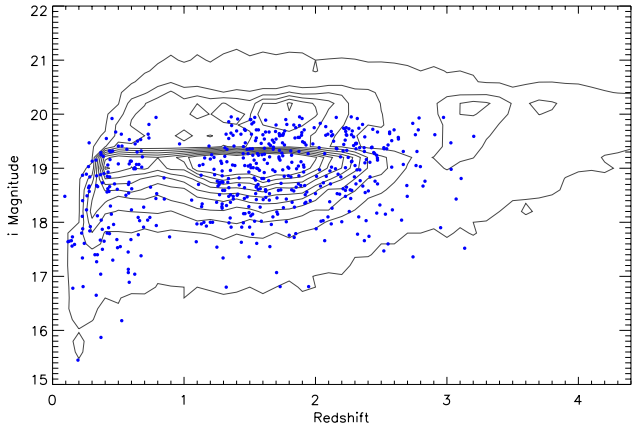

Figure 5. Redshift vs. *i*-band magnitude distributions of the 532 LAMOST detected quasars in 2011 (blue points). The contours represent the redshift vs. *i*-band magnitude distributions of the SDSS DR7 quasars. The steep gradients at $i \approx 19.1$ and $i \approx 20.2$ are due to the magnitude limits of the SDSS selection algorithms for the low- and high-redshift quasars; the low number density at $z \sim 2.7$ is caused by the degeneracy of the SDSS color of stars and colors of quasars near this redshift.

(A color version of this figure is available in the online journal.)

N V, Si IV, and C IV resonant lines as well as the C III] λ1908 line become visible. For quasars near the $z \sim 0.9$ trough, only the Mg II λ2800 line is easily detectable, other emission lines such as Hδ, Hγ, and Hβ are all redshifted to wavelengths longer than 7000 Å, where the spectra are seriously contaminated by telluric emission lines. The difficulty remains until the redshift reaches $z \sim 1.1$ when the C III] λ1908 becomes visible. At redshifts ∼2.1, although there are three emission lines, the C IV λ1549, C III] λ1908, and Mg II λ2800 lines fall in the optical, the C III] λ1908 line is unfortunately redshifted to a wavelength of 5900 Å, the crossover wavelength of the dichroic where the instrument has a very low throughput, and the Mg II λ2800 is redshifted to a wavelength ∼8700 Å where sky emission lines dominate the region. For the 213 "probable" quasar candidates detected in the LAMOST 2010 and 2011 data sets, either only one emission line had been detected or the spectrum was of marginal S/N. Since we were unable to discriminate the C IV λ1549 and Mg II λ2800 lines, no redshifts were provided. Figure 5 shows the distributions of quasars in redshift-magnitude space, we can see that not only the selection effects in redshift space but also the low number density of quasars for *i* band fainter than 18.0 indicates that the performance of LAMOST and the 2D pipeline need to be carefully characterized and optimized.

Figure 6 plots the spatial distribution in the ξ–η plane of all known background quasars found in the vicinity of M31 and M33, including the 526 newly identified with the LAMOST which are reported in this paper, 14 quasars discovered by the LAMOST based on earlier commissioning observations (Paper I), 75 SDSS quasars (Adelman-McCarthy et al. 2006, 2007), and 155 previously known quasars with redshifts listed in the NED archive. Here ξ and η are respectively right ascension and declination offsets relative to the optical center of M31 (Huchra et al. 1991). In Figure 6, the magenta stars denote the central positions of M31 and M33, respectively. The magenta ellipse represents the optical disk of M31 with an optical radius $R_{25} = 95.'3$ (de Vaucouleurs et al. 1991), an inclination angle $i = 77°$ and a position angle P.A. $= 35°$ (Walterbos & Kennicutt 1987). The quasars are distributed around M31 and M33, along the Giant Stellar Stream (McConnachie et al. 2009), as well as

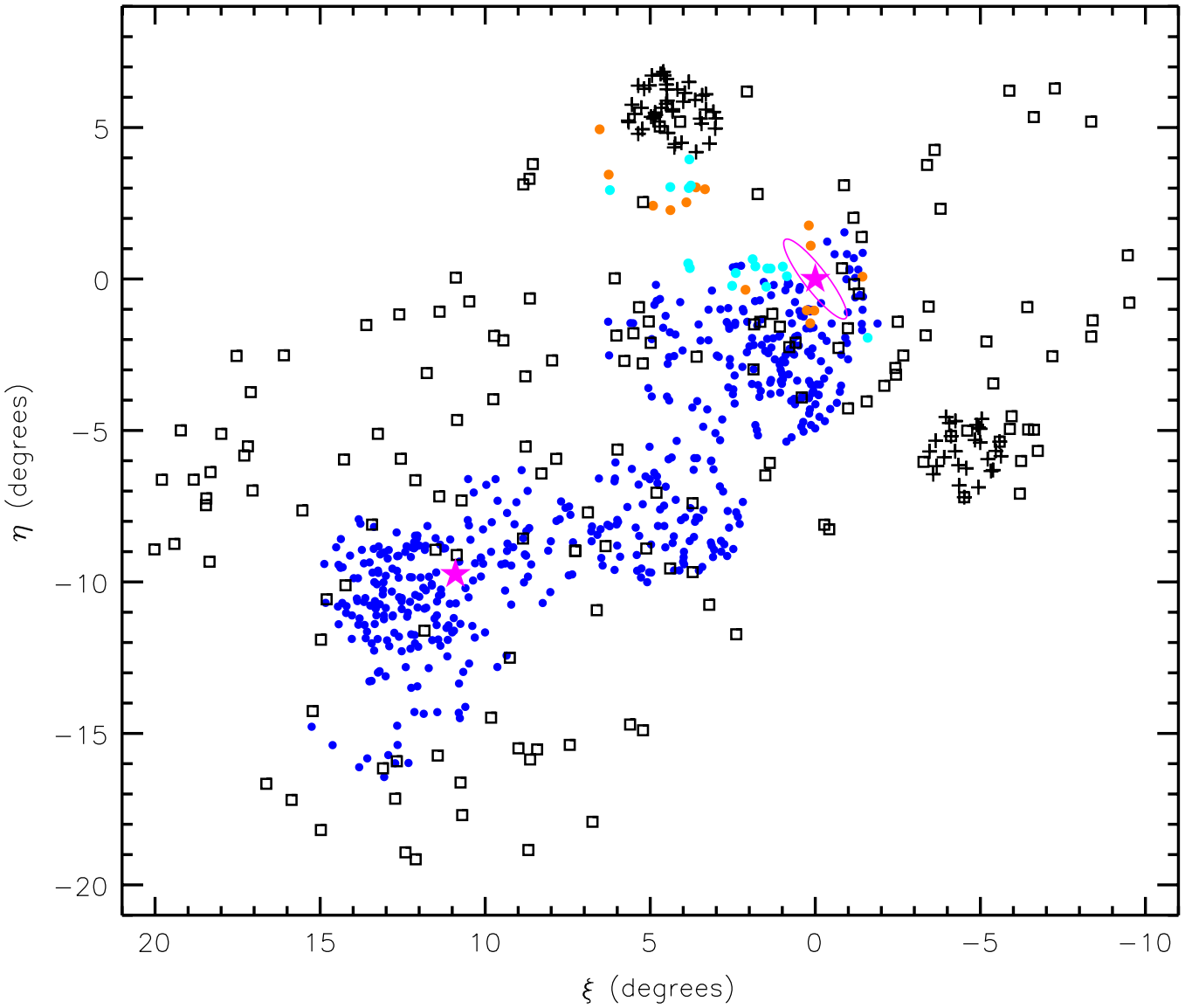

Figure 6. Spatial distributions of background quasars in the vicinity of M31 and M33. Orange, cyan, and blue filled circles represent quasars identified in the LAMOST 2009, 2010, and 2011 data sets, respectively. Crosses and open squares represent SDSS quasars and previously known quasars with redshifts archived in the NED, respectively. The magenta stars mark the central positions of M31 and M33, while the magenta ellipse represents the optical disk of M31 of radius $R_{25} = 95.'3$.

(A color version of this figure is available in the online journal.)

the extended halo of M31. Among them, there are 93 quasars within 2.°5 of M31 (about 34 kpc assuming a distance of 785 kpc to M31; McConnachie et al. 2005), 73 of them are newly discovered, 7 are from Paper I, and 13 are previously known quasars listed in the NED. Several quasars fall very close to the optical disk of M31. Tens of quasars behind the Giant Stellar Stream have been found, and the number of known quasars behind M31's extended halo and its associated substructures increases by a substantial amount. The much-enlarged number of known quasars in the vicinity of M31 and M33 should provide an invaluable sample for future PM and ISM/IGM studies of M31, M33, and the Local Group.

No quasars have been identified near the central regions of M31 and M33 due to crowding in the field. Outside those regions, the spatial distributions of identified quasars are not uniform in the 11 fields observed in 2011, one covering M33 yielded 147 quasars, giving the highest quasar number density of $\sim$7.5 deg^{-2}. On the other hand, a plate near the bottom-left corner of Figure 6 yielded only 34 quasars. The quasar number density identified by the LAMOST is lower than that of SDSS for low-redshift quasars with point-like morphology, approximately 10 deg^{-2} (Schneider et al. 2010). The low yields were mainly due to insufficient S/N, either because of poor weather conditions or lower than expected performance of LAMOST. Since the current sample of quasars was identified using the commissioning and pilot survey data, the quasar selection algorithm and telescope performance was still undergoing development and testing, and hence the sample is not homogeneous and is not intended for statistical analysis.

This work is partially supported by the Young Researcher Grant of National Astronomical Observatories, Chinese Academy of Sciences, and China Postdoctoral Science Foundation. We thank Professor Xuebing Wu and Xiaohui Fan for their careful reading and providing valuable comments and suggestions of this paper. We also thank Dr. Stephen Justham for improving the writing of the paper.

The Guoshoujing Telescope (the Large Sky Area Multi-Object Fiber Spectroscopic Telescope, LAMOST) is a National Major Scientific Project built by the Chinese Academy of Sciences. Funding for the project has been provided by the National Development and Reform Commission. LAMOST is operated and managed by the National Astronomical Observatories, Chinese Academy of Sciences.

Funding for SDSS and SDSS-II has been provided by the Alfred P. Sloan Foundation, the Participating Institutions, the National Science Foundation, the U.S. Department of Energy, the National Aeronautics and Space Administration, the Japanese Monbukagakusho, the Max Planck Society, and the Higher Education Funding Council for England. The SDSS Web site is http://www.sdss.org/.

This publication makes use of data products from *WISE*, which is a joint project of the University of California, Los Angeles, and the Jet Propulsion Laboratory/California Institute of Technology, funded by the National Aeronautics and Space Administration.

This research has made use of the NASA/IPAC Extragalactic Database (NED) which is operated by the Jet Propulsion Laboratory, California Institute of Technology, under contract with the National Aeronautics and Space Administration.

REFERENCES

Adelman-McCarthy, J. K., Agüeros, M. A., Allam, S. S., et al. 2006, ApJS, 162, 38
Adelman-McCarthy, J. K., Agüeros, M. A., Allam, S. S., et al. 2007, ApJS, 172, 634
Aihara, H., Allende Prieto, C., An, D., et al. 2011, ApJS, 193, 29
Binney, J., & Tremaine, S. 1987, Galactic Dynamics (Princeton, NJ: Princeton Univ. Press), 747
Brunthaler, A., Reid, M. J., Falcke, H., Greenhill, L. J., & Henkel, C. 2005, Sci, 307, 1440
Chemin, L., Carignan, C., & Foster, T. 2009, ApJ, 705, 1395
Crampton, D., Gussie, G., Cowley, A. P., & Schmidtke, P. C. 1997, AJ, 114, 2353
Cui, X., Su, D., Li, G., et al. 2004, Proc. SPIE, 5489, 974
Cui, X., Su, D.-Q., Wang, Y.-N., et al. 2010, Proc. SPIE, 7733, 7
Cui, X.-Q., Zhao, Y.-H., Chu, Y.-Q., et al. 2012, RAA, 12, 1197
Darling, J. 2011, ApJL, 732, L2
de Vaucouleurs, G., de Vaucouleurs, A., Corwin, H. G., Jr., et al. 1991, Third Reference Catalogue of Bright Galaxies (New York: Springer)
Fan, X. 1999, AJ, 117, 2528
Gilbert, K. M., Guhathakurta, P., Kollipara, P., et al. 2009, ApJ, 705, 1275
Huchra, J. P., Brodie, J. P., & Kent, S. M. 1991, ApJ, 370, 495
Huo, Z.-Y., Liu, X.-W., Yuan, H.-B., et al. 2010, RAA, 10, 612
Ibata, R., Chapman, S., Ferguson, A. M. N., et al. 2005, ApJ, 634, 287
Ibata, R., Martin, N. F., Irwin, M. J., et al. 2007, ApJ, 671, 1591
Jester, S., Schneider, D. P., Richards, G. T., et al. 2005, AJ, 130, 873
Kim, D.-W., Protopapas, P., Trichas, M., et al. 2012, ApJ, 747, 107
Kozłowski, S., Kochanek, C. S., Jacyszyn, A. M., et al. 2012, ApJ, 746, 27
Loeb, A., Reid, M. J., Brunthaler, A., & Falcke, H. 2005, ApJ, 633, 894
Luo, A.-L., Zhang, H.-T., Zhao, Y.-H., et al. 2012, RAA, 12, 1243
Luo, A.-L., Zhang, Y.-X., & Zhao, Y.-H. 2004, Proc. SPIE, 5496, 756
Massey, P., Olsen, K. A. G., Hodge, P. W., et al. 2006, AJ, 131, 2478
McConnachie, A. W., Irwin, M. J., Ferguson, A. M. N., et al. 2005, MNRAS, 356, 979
McConnachie, A. W., Irwin, M. J., Ibata, R. J., et al. 2009, Natur, 461, 66
Richards, G. T., Fan, X., Newberg, H. J., et al. 2002, AJ, 123, 2945
Richards, G. T., Fan, X., Schneider, D. P., et al. 2001, AJ, 121, 2308
Savage, B. D., Wakker, B., Jannuzi, B. T., et al. 2000, ApJS, 129, 563
Schlegel, D. J., Finkbeiner, D. P., & Davis, M. 1998, ApJ, 500, 525
Schneider, D. P., Hartig, G. F., Jannuzi, B. T., et al. 1993, ApJS, 87, 45
Schneider, D. P., Richards, G. T., Hall, P. B., et al. 2010, AJ, 139, 2360
Sohn, S. T., Anderson, J., & van der Marel, R. P. 2012, ApJ, 753, 7
Stern, D., Assef, R. J., Benford, D. J., et al. 2012, ApJ, 753, 30
Su, D. Q., Cui, X., Wang, Y., & Yao, Z. 1998, Proc. SPIE, 3352, 76
Tinney, C. G. 1999, MNRAS, 303, 565
Tinney, C. G., Da Costa, G. S., & Zinnecker, H. 1997, MNRAS, 285, 111
van der Marel, R. P., & Guhathakurta, P. 2008, ApJ, 678, 187
Walterbos, R. A. M., & Kennicutt, R. C., Jr. 1987, A&AS, 69, 311
Wang, S.-G., Su, D.-Q., Chu, Y.-Q., Cui, X., & Wang, Y.-N. 1996, ApOpt, 35, 5155
Wright, E. L., Eisenhardt, P. R. M., Mainzer, A. K., et al. 2010, AJ, 140, 1868
Wu, X.-B., Hao, G., Jia, Z., Zhang, Y., & Peng, N. 2012, AJ, 144, 49
Xing, X., Zhai, C., Du, H., et al. 1998, Proc. SPIE, 3352, 839
Yan, L., Donoso, E., Tsai, C.-W., et al. 2013, AJ, 145, 55
York, D. G., Adelman, J., Anderson, J. E., Jr., et al. 2000, AJ, 120, 1579
Zhao, G., Zhao, Y.-H., Chu, Y.-Q., Jing, Y.-P., & Deng, L.-C. 2012, RAA, 12, 723
Zhao, Y. 2000, Proc. SPIE, 4010, 290
Zhu, Y., Hu, Z., Zhang, Q., Wang, L., & Wang, J. 2006, Proc. SPIE, 6269, 20